IOPscience iopscience.iop.org

Home Search Collections Journals About Contact us My IOPscience

Electron paramagnetic resonance of electronic-grade SiC substrates

This article has been downloaded from IOPscience. Please scroll down to see the full text article.

2004 J. Phys.: Condens. Matter 16 R1341

(http://iopscience.iop.org/0953-8984/16/46/R02)

View the table of contents for this issue, or go to the journal homepage for more

Download details:
IP Address: 129.252.86.83
The article was downloaded on 27/05/2010 at 19:03

Please note that terms and conditions apply.

J. Phys.: Condens. Matter **16** (2004) R1341–R1367 PII: S0953-8984(04)75431-4

TOPICAL REVIEW

Electron paramagnetic resonance of electronic-grade SiC substrates

Mary Ellen Zvanut

Department of Physics, University of Alabama at Birmingham, 1530 3rd Avenue S, Birmingham, AL 35294-1170, USA

E-mail: mezvanut@uab.edu

Received 12 July 2004, in final form 24 August 2004
Published 5 November 2004
Online at stacks.iop.org/JPhysCM/16/R1341
doi:10.1088/0953-8984/16/46/R02

Abstract
Electron paramagnetic resonance (EPR) spectroscopy is a powerful tool to study the physical and chemical structure of point defects in crystalline semiconductors. Investigations throughout the past few decades have provided detailed descriptions of some of the most important intrinsic defects and impurities in silicon carbide. Several reviews have summarized the significant findings. This review expands the scope of earlier work by focusing on EPR studies of as-grown electronic grade SiC. Because the most recent technological interests focus on growing high-resistivity substrates for high frequency, high power devices, many of the defects discussed here are identified in semi-insulating 4H SiC. The access to high purity material has enabled the identification of at least one new centre, the positively charged carbon vacancy, while the detailed electronic structure of the others is still uncertain. Intentional and unintentional impurities also play a role. For this reason, vanadium and some shallow impurities will be briefly reviewed. Finally, the structure and chemistry of carbon-related defects thought to be located near the surface of SiC will be summarized.

Contents

1. Introduction 1342
1.1. The technique 1343
1.2. Overview of the defects 1346
1.3. Significance to electronic materials 1346
2. Instrinsic defects 1348
2.1. Identified defect structures 1348
2.2. Unidentified defects 1355
2.3. Role of intrinsic defects in SI SiC: defect level and thermal stability 1356

0953-8984/04/461341+27$30.00 © 2004 IOP Publishing Ltd Printed in the UK

3. Impurity-related defects 1359
3.1. Shallow impurities 1359
3.2. Deep level impurity: vanadium 1359
4. Surface and interface defects 1361
4.1. Heat-treated surfaces 1362
4.2. SiC/SiO_2 interface 1363
5. Concluding comments 1365
Acknowledgments 1365
References 1365

1. Introduction

Electron paramagnetic resonance (EPR) studies of SiC include n- and p-type material of many different polytypes. Although decades of SiC studies have produced libraries of literature covering a wide range of defects, the SiC substrates being produced today for electronic applications have yielded many new results. These are the focus of this review. In addition, because SiC is now considered one of the most promising materials for use in high power/high frequency electronics, the defects observed in device quality SiC and their relevance to the application of the material are emphasized.

SiC may be grown in many different lattice types, and only 3C lends itself to relatively simple analysis. The most commonly used polytypes today are 4H and 6H, each of which is hexagonal; they contain two (4H) or three (6H) different symmetry sites. The former has one cubic site and one hexagonal site, while the latter has two cubic sites and one hexagonal site. Note that at the cubic site, the two sets of basal bonds are mirror images of each other, as seen in figure 1(a), whereas in the hexagonal site one set is rotated 60° with respect the other, as shown in figure 1(b). These sites differ only in the orientation of the second nearest neighbours; nevertheless, most of the EPR centres identified in SiC may be distinguished according to lattice sites by symmetry and energy considerations.

In addition to electron paramagnetic resonance spectroscopy, electron nuclear double resonance (ENDOR), optically detected magnetic resonance (ODMR), and electrically detected magnetic resonance (EDMR) have been valuable tools for confirming the chemical and physical structure of point defects in SiC. Although not the focus of this article, their importance in identifying the detailed structure of the point defects addressed herein are referenced as appropriate. More recently, electron spin echo and high magnetic field experiments have provided detailed pictures of a variety of centres. A complete, well-accepted description of any defect requires years of investigations and the inclusion of non-magnetic resonance techniques as well.

The review is divided into five sections. Section 1 outlines the basics of EPR and briefly reviews the significance of using EPR to study device quality material. The next two sections focus on specific point defects, with section 2 covering intrinsic centres in the bulk of high purity substrates and section 3 reviewing some of the new information concerning the shallow donors and acceptors. The latter section also summarizes recent work related to vanadium, a deep level impurity that is intentionally incorporated into SiC to provide electrical compensation. Note that throughout this review, the term 'defect' will be used to refer to both intrinsic centres, like dangling bonds and vacancies, and extrinsic centres, such as impurities. In section 4, surface defects and those thought to be located at the SiO_2/SiC interface are discussed. Finally, the present state of knowledge concerning the complicated issue of point defects in SiC is summarized.

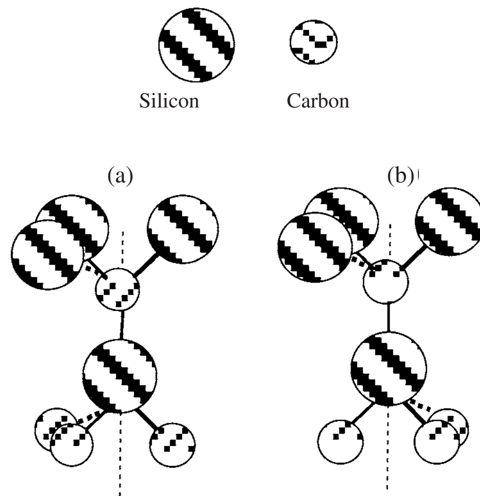

Figure 1. Hexagonal (a) and cubic (b) lattice sites in 4H and 6H SiC. In (b) the three basal carbon atoms are rotated 60° with respect to the three basal Si atoms above.

1.1. The technique

Electron paramagnetic resonance is based on the absorption of energy between spin states induced by the presence of an applied magnetic field [1–3]. If there were no internal fields affecting the defect, the absorbed energy may be described by the interaction of the applied magnetic field, B_0, with the electron spin at the defect. The appropriate Hamiltonian for this situation is:

$$H = \mu_B \vec{S} \cdot \overleftrightarrow{g} \cdot \vec{B} \tag{1}$$

where μ_B is the Bohr magneton, S is the total spin of the electron and B is the applied magnetic field. The g-tensor is related to the proportionality factor between the quantized electron magnetic dipole moment and total angular momentum. The energy solutions are the Zeeman energies for a spin 1/2 particle:

$$E = \mu_B g B m_s \tag{2}$$

where m_s is the z-component of the spin angular momentum. In the simple case of one electron free from the influence of any nuclear magnetic fields, the g-value is the Landé free electron value shifted by an amount that depends on the local environment of the defect. The shift is generally caused by a small amount of angular momentum that is not included in equation (1), but enters as a perturbation and is incorporated into the 'g' value. Thus, each defect has a characteristic g-tensor determined by its surroundings. The tensor is obtained from the g-value measured at each orientation of the sample with respect to the incident magnetic field.

The applied magnetic field is one of many such fields experienced by the electron. Both the surrounding nuclei and other electrons contribute fields that alter the energy of the electron. For most defects in SiC, the Hamiltonian may be adequately described by the following:

$$H = \mu_B \vec{S} \cdot \overleftrightarrow{g} \cdot \vec{B} + \sum_j \vec{S} \cdot \overleftrightarrow{A} \cdot \vec{I} + \vec{S} \cdot \overleftrightarrow{D} \cdot \vec{S}. \tag{3}$$

A is the nuclear hyperfine tensor representing the strength of the interaction between the electron and nuclear spins, and I is the nuclear spin. The last term represents the interaction

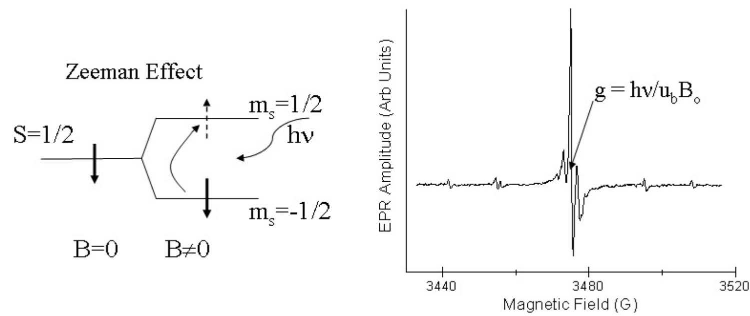

Figure 2. Energy levels of an electron split by application of a magnetic field according to the Zeeman effect. $h\nu$ represents the incident radiation required to change the spin polarity of the electron. On the right, an EPR spectrum where the resonance condition for the spin 1/2 electron, $h\nu = \mu_B g B_0$, is represented by the sharp line in the centre.

among individual spins and must be included whenever the defect represents a multi-electron centre. The spin–spin interaction may take the form of electron exchange, spin–orbit coupling, and/or electron dipole–dipole interaction. For this review, discussion will be limited to centres with $S \leqslant 1$. Thus, although a general situation demands the addition of higher order terms, equation (3) will be sufficient for all the analysis presented here.

In a standard EPR experiment, the sample is placed in the centre of a resonant cavity containing an oscillating magnetic field, and a magnetic field is applied to separate the different spin states. As equation (2) shows, the energy difference between the states, ΔE, is proportional to B; therefore, ramping the magnetic field allows one to search for the field at which absorption of the μ wave energy ($h\nu$) at a specific defect will occur. The resonance condition for a spin 1/2 centre, $\Delta E = h\nu = \mu_B g B$, is shown schematically in figure 2 (left), and a typical spectrum illustrating detection of the EPR signal at resonance is shown in figure 2 (right). Phase sensitive detection is almost always used in EPR spectroscopy so that the low number of paramagnetic centres typical of many materials may be detected. This ac detection method results in the derivative of the absorption as shown in figure 2. A very useful feature for studying many centres in SiC is that the resonance field is proportional to the microwave frequency. Therefore, resolution may be improved by performing the experiment at large microwave frequencies. Although more tedious, experiments employing frequencies as high as 250 GHz have been performed, and defects in SiC with nearly the same g-tensor have been resolved [4].

When nuclei of non-zero nuclear spin are sufficiently close to the defect, the second term in equation (3) enters, and the local nuclear magnetic field further splits the electronic levels. Since the selection rule allows only transitions with $\Delta m_s = \pm 1$, the Zeeman EPR line will divide into $2I + 1$ lines. All the hyperfine lines will have the same intensity, and they will be spaced equally from the central EPR line. Because the intensity of a transition depends on the total number of defects causing the absorption, the isotopic abundance of the non-zero spin nuclei and number of like nuclei determine the ratio of hyperfine line intensity to the Zeeman plus hyperfine intensities. The natural abundances of the ^{29}Si and ^{13}C nuclei are only 4.9% and 1.1%, making the nuclear hyperfine for intrinsic defects difficult to detect. This is illustrated by the small satellite lines on either side of the central line in figure 2.

When more than one electron is interacting at the defect, the fine structure term must be included. Often, the $M_s = 0$ state of an $S = 1$ centre is separated from the $M_s = \pm 1$ states even at zero magnetic field. This situation is referred to as the zero-field splitting. Depending on the

population of each level, the EPR spectra may consist of one absorption and one emission line or two absorption lines. Sometimes a replica spectrum may be seen at half the centre magnetic field of the $\Delta M_s = \pm 1$ lines. The 'half-field line' represents the $\Delta M_s = \pm 2$ transition.

In general, both the hyperfine term and zero-field splitting term may be required to describe the EPR spectrum. A full quantum mechanical treatment of such situations, as well as the solution under various approximating conditions, is given in [1–3]. From the discussion so far, however, it is not obvious how one uses the above information to describe the detailed structure of an intrinsic defect or impurity. Part of the picture may be gleaned directly from the spectrum. For instance, the number of nuclear hyperfine lines and their intensity relative to the Zeeman line often indicate the type and number of nuclei. The spin state may be determined by counting related EPR lines, where the number of lines should equal $2S$. Often this establishes the charge state, once the chemical nature of the centre is known. Finally, the angular dependence of the EPR spectrum, which provides the complete g- and A-tensors as well as D, provides the local symmetry of the defect. The method of distinguishing between isotropic, axial, or orthorhombic symmetry is straightforward and is described in many texts [3]. The addition of computer codes to solve the Hamiltonian and knowledge of the crystal rotation group can lead to determination of the point symmetry of the defect. Often, comparison of the measured A-tensors with the components derived from appropriate theory assists in determining which symmetry site the defect occupies as well the local symmetry of the defect itself. Unfortunately, calculations for the commonly used SiC polytypes, 4H and 6H, are difficult because the number of lattice sites required to adequately represent the unit cell is large. This has limited calculations of one of the most common impurities in SiC, the heavy transition element, vanadium. However, the intrinsic defects and light impurities such as boron and nitrogen are well studied. Predictions for their defect levels, hyperfine values, and ground state wavefunctions are available [5]. Comparisons between calculations and a wealth of experimental data have produced a very detailed picture of certain defects, as will be seen below.

Since the paramagnetic state is related to the charge state, the position of the Fermi level in the semiconductor can greatly alter the type of spectrum obtained for a specific defect. The relative position of the E_f and the defect level determines the charge state present. Vanadium, which may be present in any of three different charge states in 4H SiC, offers a good example. An energy approximately equal to 1.6 eV is necessary to add an electron from the valence band edge (E_v) to V^{5+}; the energy required to convert V^{4+} to V^{3+} is greater than $E_v + 2.26$ eV. These energies locate the defect levels, $V^{4+/5+}$ and $V^{3+/4+}$, for the vanadium impurity. If E_f is below midgap (approximately the $V^{4+/5+}$ level) no EPR signal will be seen from vanadium. As the Fermi level rises above the $V^{4+/5+}$ level, first V^{4+} will be observed then V^{3+} will be seen as the Fermi level approaches the $V^{3+/4+}$ level. In principle, an equal amount of V^{3+} and V^{4+} will be present when E_f is located at $V^{3+/4+}$. Finally, as E_f approaches the conduction band edge, only the V^{3+} EPR signal will be observed. Such a scenario will apply to any defect with a level or levels in the bandgap.

As suggested by the above discussion, in the as-grown crystal not all defects are paramagnetic as required for detection by electron paramagnetic resonance. Illumination of the sample with a standard lamp/monochrometer system using wavelengths from the near infrared to near ultraviolet is commonly used to induce paramagnetic states. One of two situations may result. Diamagnetic ($S = 0$) centres may be excited to their triplet ($S = 1$) state where the $\Delta M_s = 1$ transitions within the $S = 1$ manifold may be seen. The spin state is deduced by the presence of $2S$ number of lines and the lower probability $\Delta M_s = 2$ transition ('half-field' lines). Both the carbon vacancy–carbon antisite (V_C–C_{Si}) pair and silicon vacancy are identified in SiC using this method. In general, any high spin state of the defect accessible

to the excitation energy may be induced. The other scenario that may develop is that an electron is removed from the defect to the conduction band, or captured by the defect after carrier excitation from the valence band. A less likely possibility is defect-to-defect electron transfer. Ionization of centres not only enables detection of previously compensated sites, but may lead to determination of the electrical level of the defect. For instance, the $V^{4+/5+}$ level was found to be 1.6 eV above the valence band edge, E_v, using photo-induced EPR [6]. More recently, the plus-to-neutral level for the carbon vacancy, V_C, was also reported [7, 8].

1.2. Overview of the defects

An enormous number of SiC EPR studies exist, making it impossible to review all of the defects previously identified as well as the many more spectra that remain unidentified. Studies include both the shallow and deep impurities in 3C, 4H, 6H and, less frequently, 15R polytypes [5, 6, 9–12]. The radiation-induced intrinsic defects identified to date include the silicon and carbon vacancies, several vacancy complexes, and possibly V_C–H pairs. Recent studies of 4H and 6H high purity material used for electronic applications have sparked new interest in the well-studied impurities as well as the intrinsic defects. In addition, the importance of surface defects for device processing has initiated EPR studies of near-surface and interfacial centres.

The intrinsic defects identified to date in as-grown electronic-grade 4H SiC are listed in the first column of table 1. The remaining columns give the EPR parameters measured for each defect, a descriptive model of the defect, the temperature at which the values were obtained, and reference details. Most centres have been studied at several temperatures; the temperature reported here is the one for which the most complete set of parameters is available. The temperature dependence of the g-tensor, hyperfine constants, and fine structure factors are discussed below. All of the parameters were obtained from irradiated SiC except those listed for the last two centres. P6 and P7 were obtained from studies of 6H SiC, but similar parameters were reported recently in as-grown 4H SiC [13, 14].

1.3. Significance to electronic materials

In electronic materials, knowledge of the defect charge state and the number of defects in a particular charge state is critical. EPR focuses on defects in a specific charge state so that both the type and number of centres may be determined. For example, both the commonly seen shallow boron acceptor and nitrogen donor may be detected in the neutral state only. In addition, since the change in charge state may be observed by monitoring the signal intensity due to a specific centre, the kinetics of passivation by other impurities may be monitored. Also, photo-induced EPR may change the charge of the defect and enable determination of the defect level.

One of the most important pieces of information to those interested in device properties of the material is the concentration of a specific defect. In many cases, the total number of centres in a specific charge state may be determined by EPR through a comparison of the spectrum of the desired centre with that of a standard. Although straightforward for the simple spin $1/2$ defects, the counting process becomes significantly more complicated for high spin centres in the large crystal field often present in hexagonal SiC. Nevertheless, with proper care, the total number of centres may still be determined. Unless otherwise stated, the concentration is based on the assumption that the defects are uniformly distributed throughout the sample. For the small pieces of $1/2$ mm thick samples usually used for EPR studies, the resulting concentration number is reasonably reliable.

Table 1. Defects identified in as-grown SiC (parameters obtained from centres in irradiated material).

		EPR parameters									
		g-tensor			Fine structure (MHz)		Hyperfine (MHz)				
Centre	S	g_x	g_y	g_z	D	E	$A_{\parallel}$	$A_{\perp}$	Model	Temp (K)	Reference
P_{6a}	1	2.004 4	2.004 4	2.003 5	1368						
P_{6b}	1	2.004 4	2.004 4	2.034	1341	0			V_C–C_{Si}		
P_{6c}	1	2.004 8	2.004 8	2.003 6	1290	0	C: 48	—	C-axis	7	[23, 24]
P_{7a}	1	2.004 8	2.004 8	2.003 5	1347	−4	Si: 12	—	V_C–C_{Si}		
P_{7b}	1	2.004 8	2.004 8	2.003 5	1323	46			Basal bonds		
P_{7c}	1	2.004 4	2.004 4	2.003 4	1248	−1					
	1				35.1		C1: 80.3	34.8			
T_{V2a}	or	2.002 9	2.002 9	2.002 9	($S = 3/2$)	0	C2-4: 75.8	31.3, 27.2	V_{Si}	160	[15, 18, 19],
	3/2				70.1		Si: 8.7	8.7			
					($S = 1$)						
							Si1: 181.8	125.2			
EI5	1/2	2.004 84	2.004 84	2.003 22	—	—	Si2-4: 145.1	101.7	V_C^+, cubic site	150	[26, 27, 32]
							NNN: 11.2	8.13			
							Si1: 365.9	251.3			
EI6	1/2	2.004 72	2.004 72	2.003 05	—	—	Si2-4: 83.2	56.3	V_C^+, hex site	150	[4, 31, 32]
							NNN: 21.0	16.5			
		2.003 2	2.003 2	2.002 3	—	—	C: 219	105	C-dangling		
P_{bC} [a]	1/2	2.003 1	2.002 8	2.002 3			Si: 36.4	36.4	bond at	300	[60]
									SiC/SiO_2 IF		
[a]	1/2	2.002 4	2.002 4	2.002 4	—	—			C-dangling		
									bond near	300	[40, 41]
									SiC/SiO_2 IF		

[a] Only studied in as-grown material.

2. Instrinsic defects

This section reviews the intrinsic defects observed in as-grown electronic grade SiC. First, those for which the structure has been previously identified in material irradiated by high energy particles are discussed. Then, spectra associated with several as-yet unidentified centres are reviewed. Here, as well as in the next section, results obtained from the 4H polytype are emphasized. To avoid repetition, SiC will imply 4H material, and other polytypes are noted as appropriate.

2.1. Identified defect structures

Until recently, there were very few reports of defects in bulk as-grown hexagonal SiC. Generally, high energy particle irradiation is employed to enhance the typically low number of intrinsic defects. Indeed, it is from irradiation studies that most of the detailed description of the intrinsic centres arises. As of this writing, at least three of the defects previously identified in irradiated samples have been identified in as-grown SiC wafers: a silicon vacancy (V_{Si}), the doubly positive charged carbon vacancy–carbon antisite pair $(V_C–C_{Si})^{2+}$, and a positively charged carbon vacancy (V_C^+). In as-grown material, the defects addressed below are seen exclusively in semi-insulating (SI) wafers, suggesting that the paramagnetic charge state lies energetically deep within the band gap.

Silicon vacancy, V_{Si}. At least two types of spectra are identified as Si vacancy-related centres in SiC. One consists of a single, isotropic line at $g = 2.0028$–2.0034 [15–17]. The nuclear hyperfine tensor agrees well with that predicted for the negative charge state of the silicon vacancy [16, 17]. Furthermore, pulsed EPR studies have confirmed that it represents a spin $3/2$ centre at a site of high symmetry, thus eliminating the zero-field splitting that can occur for high spin defects [15, 16]. V_{Si}^- has not been observed in as-grown SI 4H or 6H substrates, suggesting that the neutral-to-negative transition lies in the upper half of the band gap. The second type of spectrum, labelled T_{V2a} in figure 3, is observed in semi-insulating SiC wafers grown by either physical vapour transport (PVT) or high temperature chemical vapour deposition (HTCVD) [18]. The lines marked a, b, and c represent the central line and two sets of hyperfine lines, respectively. The remaining signals in the figure will be discussed later in this review. Using irradiated samples with much larger signal intensity, several groups measured the angular dependence of the hyperfine lines and determined the g- and A-tensors and fine structure listed in table 1. Analysis revealed a defect with 12 next nearest neighbour (NNN) Si and 4 nearest neighbour (NN) C atoms, indicating that the spectrum is due to an Si vacancy in which most of the electron wavefunction (63.2%) is concentrated at the carbons, while only 2.3% is on the next nearest neighbours [15, 19]. The model is shown in figure 4, where the hatched circles represent Si, and the smaller shaded circles carbon. The multi-line nature of the spectrum and the angular dependence of their line positions imply that the defect state has electron spin $>1/2$. The observation of the spectrum under equilibrium conditions indicates that the ground state of the defect is a high spin state, in agreement with theoretical calculations for Si vacancies in hexagonal SiC [20]. In addition to the studies of Son and co-workers, Orlinski, and separately Von Bardeleben, show that the EPR lines can be observed at 4 K without external illumination [16, 21]. The temperature-dependent studies performed by Mizuochi and co-workers and ESE studies of Orlinski also support conclusion of a high spin ground state [15, 16].

Although there is considerable understanding of the defect structure, there is no consensus with regard to the spin state of the centre. The uncertainty arises because the pair of lines

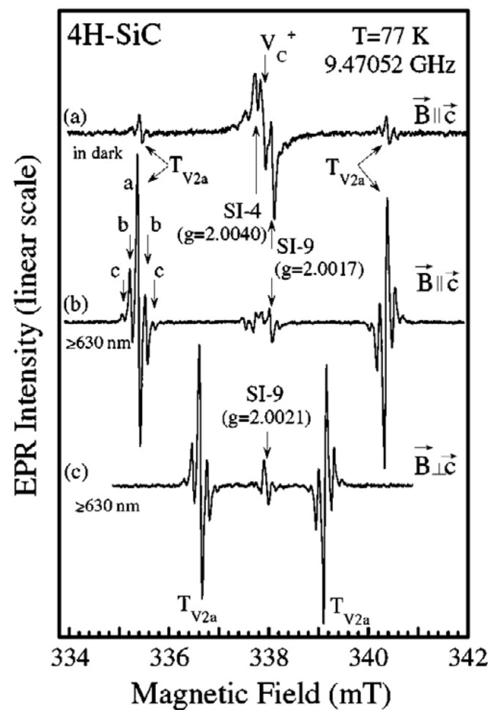

Figure 3. EPR spectrum measured in as-grown 4H SiC before (a) and after, (b), (c), illumination with sub-band gap light. Lines marked T_{V2a} represent V_{Si}, where 'a' represents the Zeeman line; 'b' and 'c' arise from the 1 and 2 NNN Si atoms, respectively. The defects represented by SI-4 and SI-9 have not yet been identified. (Reprinted figure with permission from Son *et al* [18], copyright 2003 by the American Physical Society).

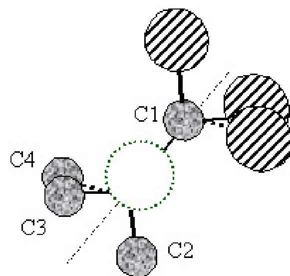

Figure 4. Model of V_{Si}. The dashed line represents the *c*-axis; the small grey circles are carbon atoms; the larger hatched circles are Si atoms. The unfilled dashed circle marks the missing Si atom.

identified in figure 3(a) as T_{V2a} is always accompanied by a strong line positioned precisely where one might expect a third line from a spin 3/2 defect. Additional studies are unable to convincingly determine whether the central line belongs to the outside pair or represents an unrelated centre. Note that the central line occurs at $g = 2$, where many common single-line spectra occur, particularly in carbon-based materials. Employing the nutation method afforded by pulsed EPR measurements, Mizuochi and co-workers directly detected the different ΔM_s transitions [15]. Their data suggest that the centre represents a defect with electron spin 3/2. On the other hand, Orlinski and co-workers used a method based on the optimal pulse length for

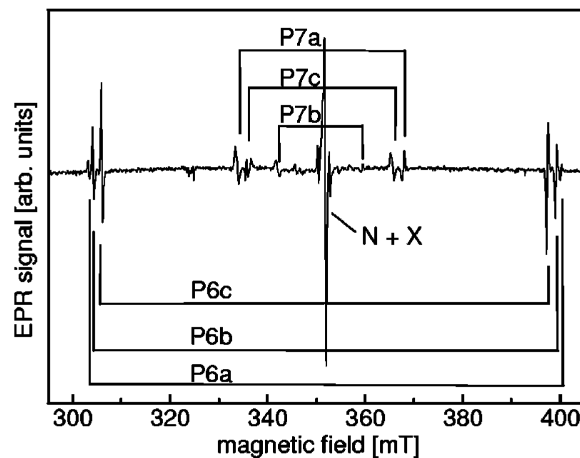

Figure 5. EPR spectrum of P6 and P7 centres obtained from neutron-irradiated 6H SiC with the magnetic field oriented parallel to the *c*-axis. (Reprinted figure with permission from Lingner *et al* [23], copyright 2001 by the American Physical Society).

an electron spin echo signal and concluded that the defect represents an $S = 1$ centre [16]. The standard continuous wave EPR studies of Son and co-workers support the latter conclusion, as is illustrated in figures 3(b) and (c), which depict spectra obtained with B parallel (figure 3(b)) and perpendicular (figure 3(c)) to the c-axis after illumination with light of wavelength less than 630 nm [18]. The intensity of the two lines labelled T_{V2a} is greatly enhanced with respect to the central line when the sample is illuminated with wavelength less than 630 nm. The authors present a defect level scheme for an $S = 1$ centre in which optical excitation preferentially occupies the (1, 0) level after de-excitation from the singlet state [18]. With this level more highly filled than the (1, 1) and (1, −1) states, the $M_s = 0$ to 1 and $M_s = 0$ to -1 transitions occur with greater probability than prior to illumination. Thus, the intensity of the two EPR lines increases with illumination, and the phase of each is opposite, as is consistent with stimulated absorption when M_s changes from 0 to 1 and stimulated emission when M_s changes from 0 to −1. Although Son's argument is very convincing, Mizuochi and co-workers present a case involving polarization-dependent excitation of spin 3/2 centres which, although more complicated, must be considered [15]. Until the outer lines of T_{V2a} are observed without the confusing central line or additional time-dependent EPR studies are performed, the spin state of this silicon vacancy centre remains uncertain. Significant to the role of the defect in electronic materials, the inability to determine the electron spin multiplicity means that the charge state is not yet determined. T_{V2a} represents either a second negatively charged vacancy, V_{Si}^{-}, or the neutral charge state, V_{Si}^{0}. As will be discussed below, the charge state, or even the defect itself, may not be as important as several other intrinsic defects in compensation of SI SiC because V_{Si} is thought to be unstable at high temperature [11, 14, 22]. Indeed, since the annealing mechanism of V_{Si} likely involves capture of a nearby C atom to form a V_C–C_{Si} pair, the role of the silicon vacancy may primarily be as a precursor for the defect pair described below.

Carbon vacancy–carbon antisite pair, V_C–C_{Si}. The EPR spectrum of V_C–C_{Si}, shown in figure 5, was obtained on neutron-irradiated 6H SiC annealed at 1000 °C with the magnetic field parallel to the c-axis [23]. The lines labelled P6 and P7 were reported earlier by Vainer and Il'in

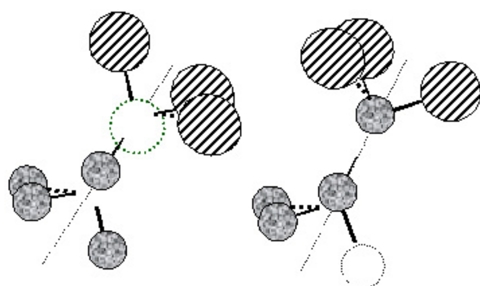

Figure 6. Model of the carbon vacancy–carbon antisite pair represented by the P6 (a) and P7 (b) EPR spectra. The dashed line represents the *c*-axis; the small grey circles are carbon atoms; the larger hatched circles are Si atoms. The unfilled dashed circle marks the missing C atom.

studying n-type 6H SiC, which was quenched during growth and subsequently annealed [24]. The lines identified as 'a', 'b', and 'c' arise from the same defect located at the three different symmetry sites in 6H SiC. Similar spectra consisting of only of the 'a' and 'c' lines are observed in 4H samples [13, 14]. The centres are generally seen after illumination with 1.1 eV light. The magnetic resonance signal was analysed in detail by Son using ODMR and Lingner with EPR [23, 25]. Most studies conclude that P6 and P7 each represent a centre with an electron spin zero ground state and $S = 1$ excited state 1.1 eV above the ground state. The symmetry of the two centres shows that the defect associated with P6 is aligned along the *c*-axis while that identified by P7 lies almost exactly along the basal bond of the tetrahedra. Based on the directions of the two principal axes and the angular dependence of the spectrum, it was concluded that P6 and P7 represent pair centres. The values for the EPR parameters are listed in table 1.

The nuclear hyperfine lines have only been studied with B parallel to the *c*-axis, so that a definitive model for the defect may not be determined. However, Lingner and co-workers have provided convincing arguments that the P6 and P7 spectra represent different orientations of a carbon vacancy–carbon antisite pair. A model for P6 is shown in figure 6(a) and P7 in figure 6(b), where the hatched circles represent Si nuclei and the filled circles indicate carbon. The model is deduced after consideration of formation energies, excited state energy levels, and hyperfine values for different types of pairs [23]. Si_C–V_{Si} is thought unlikely because calculations based on the self-consistent linear muffin tin orbitals method in the atomic spheres approximation (LMTO-ASA) predict that the pair is unstable against recombination of Si with the vacancy, leaving behind an isolated carbon vacancy. The theory is indirectly supported by frequent observations of V_C in high purity, semi-insulating SiC [7, 26]. The C_{Si}–Si_C pair is discounted because calculations show that the excited state is less than 0.2 eV above the ground state, contrary to the photon energy required to observe the P6/P7 centres. Finally, the observed hyperfine structure is inconsistent with a divacancy, V_{Si}–V_C, model. The intensity of the hyperfine lines with $A_\parallel = 48$ MHz is indicative of a carbon nucleus and that for lines with $A_\parallel = 12$ MHz could represent 4–8 Si. These data are consistent with a picture of a defect consisting of one C atom and six NNN Si atoms aligned along the *c*-axis, as is expected for the V_C–C_{Si} pair, but not a divacancy. As mentioned above, P6 and P7 represent two different orientations of the pair. For one set of lines (P6) the pair is oriented along the *c*-axis, and for the other (P7) the pair is aligned along any one of the three basal bond directions (figures 6(a) and (b), respectively). Finally, comparison of the ^{29}Si hyperfine values with those calculated for the neutral and double-plus charge states of V_C–C_{Si} pair indicates that the defect carries a charge of plus two [23].

The defect levels for the V_C–C_{Si} pair have not been measured; however, theoretical studies have determined which charge states should have levels in the band gap. The calculations show that only the double-plus and neutral states will exist because the pair exhibits a negative correlation energy [23]. The negative correlation energy implies that the carbon vacancy–carbon antisite pair is an efficient compensating defect, thus supporting the conclusion that the defect likely plays a major role in the compensation of SI SiC.

Carbon vacancy, V_C^+. The carbon vacancy was first identified in electron-irradiated 6H SiC by Bratus and co-workers and in both 4H and 6H polytypes by Son and co-workers [27, 28]. The former identified three sets of lines, Ky1, Ky2, and Ky3, which were tentatively assigned to the positively charged carbon vacancy at three inequivalent lattice sites in 6H SiC. The assignment for Ky2 is consistent with that determined for EI5 found in both hexagonal polytypes by Son and co-workers. *Ab initio* calculations based on density functional theory using either a 78 atom or 128 atom cluster show that the experimental data reflect the hyperfine tensor for a positively charged isolated carbon vacancy at a cubic site [29, 30]. A centre with spectroscopic features matching those reported for the irradiated samples was reported by Zvanut and Konovalov studying as-grown high purity 4H SiC [7, 26]. The EPR spectrum for this centre measured at 10 and 250 GHz with B parallel to the c-axis is shown in figures 7(a) and (b) respectively, where the lines labelled ID1 are those that closely approximate the spectrum for EI5. The g-tensor and A-tensor for the second feature, labelled ID2, are similar to those of EI6 and Ky3. The inset of figure 7 shows an expanded view of the barely resolved central lines for two defects measured at 10 GHz. In spectrum (b), the separation of the central Zeeman lines is sufficient to provide a clear distinction between the two different spectra and distinguishes the sets of satellite lines associated with each defect. Comparison of the 10 and 240 GHz spectra indicates that the magnetic field separation between the pairs of satellite lines does not change with frequency. This supports the identification of the lines labelled as ID1-1, -2, and -3 and ID2-1, -2, and -3 as hyperfine spectra for the associated Zeeman line. Similar spectra are now commonly detected in PVT and HTCVD SI SiC wafers.

Despite the similarity between Ky3, EI6, and ID2, they were tentatively attributed to different defects: Ky3 and ID2 to a carbon vacancy on a hexagonal site and EI6 to a silicon antisite, Si_C [4, 28, 31]. The 95 GHz studies used by Son and co-workers provided convincing evidence towards interpretation as an Si_C; however, no consideration was made of a carbon vacancy and a complete angular dependence of the hyperfine lines could not be measured. Comparing spectra obtained at 240 GHz with simulations for a carbon vacancy and an antisite, Konovalov and co-workers concluded that the hyperfine intensities more accurately reflect those of a carbon vacancy rather than an antisite. Unfortunately, identification of a defect from experimental evidence alone is based almost completely on the relative intensities of hyperfine lines with respect to the Zeeman line, values which are similar for an antisite (0.196) and carbon vacancy (0.147). Nevertheless, the simulation indicated clearly that a carbon vacancy is a possible defect assignment.

Recent measurements obtained at 95 GHz have yielded sufficient line separation and angular dependence to produce a detailed picture of both centres represented by figure 7. Umeda and co-workers measured the angular dependence for the hyperfine lines of both EI5 and EI6 at 95 GHz [32]. The A-tensor for each agrees well with the results of density functional theory calculations for V_C^+ located at the cubic (EI5) and hexagonal (EI6) sites, respectively [29]. The more recent study also included pulsed ENDOR measurement that revealed the presence of three next nearest neighbour carbon atoms for the EI6 centre. From this work, a picture of a carbon vacancy located at the two symmetry-related sites in 4H SiC emerges. A model is shown in the upper left inset of figure 7. The single dark grey circle

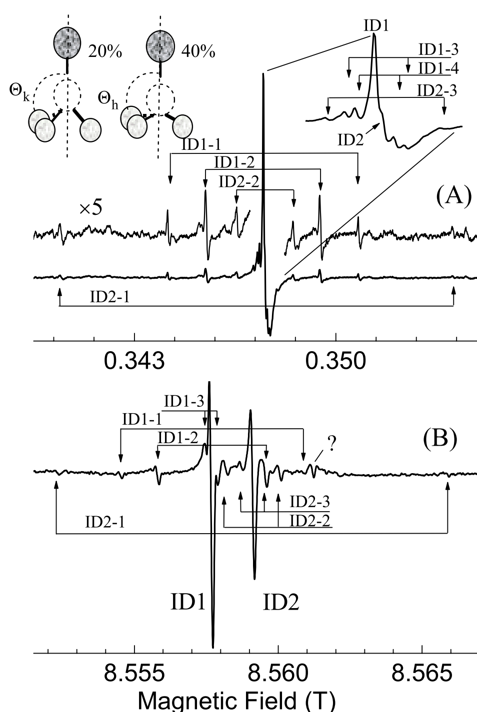

Figure 7. 10 GHz (a) and 240 GHz (b) EPR spectra of V_C^+ measured with the magnetic field parallel to the *c*-axis. ID1 and ID2 label the spectra due to the vacancy at the cubic and hexagonal sites, respectively. The inset on the upper right presents an expanded view of the central lines in the 10 GHz spectrum. The inset on the upper left illustrates a model for the carbon vacancy. The dashed circle represents the vacancy; the other four circles represent the Si nearest neighbours.

represents Si1, the axial Si nearest neighbour (NN), and the remaining lightly shaded circles represent Si2–4, the basal Si atoms. The hyperfine constants for these are shown in table 1 along with those for the next nearest neighbour (NNN) carbon nuclei. The label Θ_k identifies the cubic site, while Θ_h marks the hexagonal site. Their significance is discussed below.

The identification of EI6 with a second carbon vacancy was at first surprising, because the hyperfine splitting for the axial Si nearest neighbour for EI5 and EI6 differ by 50%. Theoretical studies show that the difference originates from a compression of the Si backbond angles at the hexagonal site compared to an extension of these same bonds at the cubic site [29]. The compression results in rehybridization of the orbitals, which produces a greater spin density on the axial Si at the hexagonal site compared to that at the cubic site, thus producing a significantly larger value for $A_{\parallel}$. The spin densities, derived from the 95 GHz EPR measurements obtained at 150 K, are labelled in figure 7. The temperature dependence of the measured hyperfine tensor offers support for the theoretical model. As shown in [32], $A_{\parallel}$ for the axial Si at the hexagonal site increases from 12.29 to 15.48 MHz between 293 and 10 K, while that for the backbonded Si decreases from 3.21 to 2.11 MHz over the same temperature range. The results are interpreted in terms of a relaxation of the Si backbonds and are consistent with an angle, Θ, between the *c*-axis and principal *A* axis, which decreases toward 90° as the temperature approaches 10 K. In figure 7, Θ_k and Θ_h represent the angles for each site, where the compression of the backbonds for the hexagonal site is exaggerated for illustration.

The symmetry of V_C at the hexagonal site is shown by both theory and experiment to be C_{3v} [29, 32]. However, the same calculations predict that V_C at the cubic site should exhibit C_{1h}

symmetry. The origin of the lower symmetry arises from a preferential pairing of two of the Si backbonds, leaving the paramagnetic electron inclined toward the remaining unpaired nucleus. Temperature-dependent EPR measurements above about 10 K indicate C_{3v}, with no evidence of the preferred orientation of the electron. However, as the temperature is lowered toward 4 K, the single EPR line for the cubic site separates into as many as three lines, indicating a lower symmetry [4, 26, 32]. Although the low temperature angular dependence has not yet been completely analysed, preliminary results are consistent with C_{1h} symmetry, as predicted. It is interesting to note the similarity of the temperature-dependent symmetry of V_C^+ with that seen for the cubic and hexagonal sites of the shallow boron acceptor [5].

Observation of an EPR active state for the carbon vacancy is somewhat surprising because earlier theoretical calculations based on *ab initio* density functional theory and the local spin-density approximation predicted a negative correlation energy for V_C [33]. The results imply that the only stable states for the carbon vacancy are the doubly positively charged state, the neutral state, and the doubly negatively charged state, all of which are non-paramagnetic. Nevertheless, as the discussion above indicates, the existence of the positively charged carbon vacancy in 4H and 6H SiC is well established. Torpo and co-workers show that the negative correlation energy may be eliminated by inclusion of a Madelung correction into the *ab initio* calculation [34]. They predict that the energy to convert a positively charged vacancy to its neutral state ($V_C^{0/+}$) is $E_v + 1.22$ eV for the cubic site and $E_v + 1.34$ eV for the hexagonal site. Similar values are determined from photo-induced EPR, a method in which the EPR signal is measured after exposure to selected photon energy [7, 8]. In as-grown high purity 4H SiC, photo-EPR measurements produced a decay in the V_C signal intensity at 1.1 eV accompanied by an approximately equal increase in the boron signal at the same photon energy [7]. Figure 8 shows the concentrations of V_C (filled squares) and B (unfilled circles), relative to their respective maximum concentration, $[X]_{max}$. Note that the maximum concentration of boron is approximately ten times that of V_C, so that the boron increase at 1.1 eV is barely detectable in this sample. If direct defect-to-defect charge transfer is assumed, the results are consistent with the 1.5 eV $V_C^{0/+}$ level recently reported for electron-irradiated p-type SiC in which the concentration of carbon vacancies was orders of magnitude greater than the intrinsic doping density for boron. The level is obtained by adding the 1.1 ± 0.2 eV V_C threshold energy to the known defect level for the boron acceptor (0.3–0.4 eV above E_v). Based on the results discussed above, it appears that the plus-to-neutral transition energy of V_C is confirmed. However, photo-induced EPR measurements of several different as-grown SI SiC wafers show variations in the optical threshold for the EPR response of V_C from 0.7 to 1.5 eV [35, 36]. Furthermore, some samples exhibit additional defects such as the two indicated in figure 8 with the plus sign and asterisk. The physical structure of these centres has not yet been identified, but they likely influence the charge transfer process. Finally, it should be pointed out that in order to completely analyse the situation, the time-dependent excitation and decay must be measured at each photon energy. In this way, a true optical cross section can be determined. The energy dependence of the cross section may then be used to locate the defect level. A cursory time-dependent study of a defect referred to as IP in SI SiC was reported by Kalabukhova and co-workers [37]. The wavelength dependence of the signal's decay after exposure to band gap illumination is consistent with the 1.5 eV defect level. However, the defect structure is not identified, and no analysis of the time dependence is provided.

One remaining problem regarding the defect level for V_C^+ is that, although the level for the plus-to-neutral transition agrees well with theoretical predictions, the present interpretation of the photo-EPR data assumes that the relaxation energy is negligible. That is, the energies for the plus-to-neutral transition ($V_C^{+/0}$) and neutral-to-plus transition ($V_C^{0/+}$) add to the band gap.

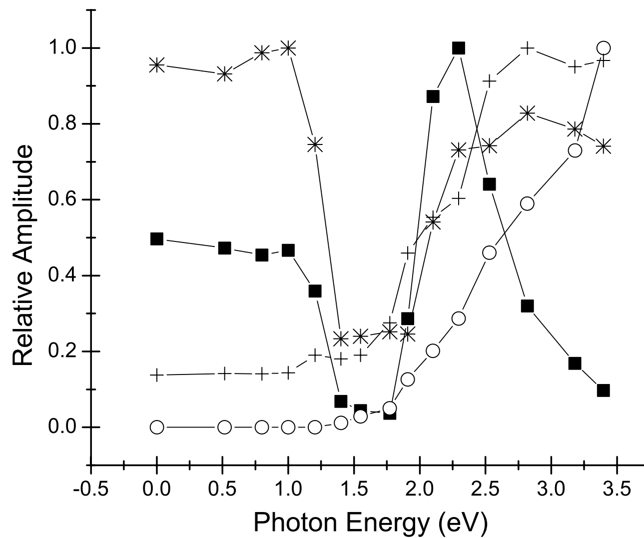

Figure 8. Photo-induced EPR data obtained from as-grown 4H high purity SI SiC. Filled squares—V_C^+; unfilled circles—shallow boron acceptor; the plus sign and asterisk represent unidentified defect structures. The intensity is measured relative to the maximum observed for each centre; the total amount of boron is about ten times that of V_C.

According to calculations, the Franck–Condon transitions for $V_C^{+/0}$ and $V_C^{0/+}$ may differ by an amount at large as 0.8 eV [38]. Thus, photo-thresholds for the two transitions should not sum to the band gap. Additional photo-induced EPR studies are in progress to address this issue.

Although V_C^+, $(V_C–C_{Si})^{2+}$, and V_{Si} are the only intrinsic centres identified in bulk as-grown SiC, it should be noted that most of the defects revealed by magnetic resonance studies of irradiated samples likely exist prior to irradiation. These include the several types of complex defects involving H or other impurities [9, 11]. As high purity, high quality material becomes more readily available, such defects will no doubt be revealed and their complex interactions with the lattice thoroughly studied.

2.2. *Unidentified defects*

EPR measurements at both 10 and 95 GHz have revealed the presence of many spectra not yet attributed to a particular defect structure. Son and co-workers report as many as nine different types of centres, referred to as SI-1 through SI-9 in PVT or HTCVD SI SiC [39]. The isotropic SI-1 with $g = 2.0026$ and no associated hyperfine lines is likely the signature of carbon broken bonds, as previously identified by several other groups [40, 41]. The remaining centres have lower symmetry, different annealing temperatures, and may be excited by varying energies of light. Further work is in progress to distinguish these centres.

A two-line spectrum with nearly isotropic g-value appears in HPSI PVT wafers recently purchased from Cree, Inc. At 77 K, the angular dependence of the separation between the two lines may be fitted to an $S = 1$ centre with $g = 2.0052$, $D = 330 \times 10^{-4}$ cm^{-1} and $E < 19 \times 10^{-4}$ cm^{-1}, similar to the P8 centre documented by Vainer and Il'in studying irradiated, annealed 6H SiC [24]. Although the angular dependence of the pair of lines is more complicated at 4 K, the increased intensity affords observation of the half-field line, confirming the spin 1 nature and nearly isotropic g-value. The centre is not observed in the dark, but appears after illumination with wavelength $<$680 nm. The photo-induced EPR results

are depicted as plus signs in figure 8. The optically induced signal is stable upon removing the light and the signal intensity increases monotonically to band-gap radiation. Such behaviour suggests that $S = 1$ is the ground state and that light provides the energy to excite the EPR active charge state.

Three sets of hyperfine lines are measurable at B parallel to the c-axis. One with a separation of 14 G is clearly resolved and two others at $\Delta B = 30$ and 41 G are barely resolved. Estimates for the ratio of the hyperfine intensity to that of the total spectrum indicate that the 14 G pair represents 12 carbon atoms and the other two signify two inequivalent sets of 4 Si nuclei, assuming a purely intrinsic defect. The only impurities that could account for the hyperfine intensity ratio are Cd, W, Hg, or Pb, all unlikely candidates in HPSI SiC. SIMS measurements have not detected any of these impurities. The large number of Si and C atoms associated with the centre suggests that the spectrum represents a complex, rather than a simple isolated defect. The fine structure parameters and A-tensor are similar to the P8 centre which was reported to be pair defect associated with nitrogen. However, Vainer and Il'in state that P8 is not photosensitive and report a nitrogen hyperfine interaction. At present, the identification of the two-line spectrum remains uncertain.

2.3. Role of intrinsic defects in SI SiC: defect level and thermal stability

All of the intrinsic defects in SiC are thought to form 'deep levels'. For wide band gap semiconductors this term refers to a charge state transition that requires energy greater than about 1 eV. These deep intrinsic defects may be deleterious in n-type and p-type SiC designed to function as active transistor components. On the other hand, in semi-insulating substrates required for high frequency transistors, the deep levels are beneficial because they neutralize the excess donors or acceptors. In both HTCVD and PVT SI SiC, the number of unintentional shallow impurities is reported to be 10^{15} and 10^{16} cm^{-3}, respectively, and it is generally assumed that the number of excess donors or acceptors is the same order of magnitude. In neither type of SiC is the uncompensated impurity concentration sufficiently low to provide the resistivity at the temperatures desired, so the material is grown in such a way as to create deep levels for compensation. It is necessary that the level be greater than 1 eV from either band edge to guarantee that the carrier remains trapped at the compensating centre at high temperature. The three defects identified earlier will be assessed with respect to their relevance to electrical compensation.

In the case of PVT substrates, at least two studies are reported that specifically address the compensating defect and its electrical level as determined by temperature-dependent Hall measurements [42, 43]. The studies were performed on samples from several SI SiC wafers grown by physical vapour transport at Cree, Inc., and were characterized before and after high temperature annealing using temperature-dependent Hall and resistivity measurements, as well as EPR. The activation energy, E_a, derived from the temperature-dependent resistivity varied between 0.9 and 1.5 eV. (Generally, the carrier concentration data were unreliable due to small fluctuations in the temperature that occurred that were of the order of the standard measurement time. Nevertheless, in all cases the Arrhenius plots for concentration provided similar E_a to those obtained from the resistivity data.) For all samples in this study, before and after annealing, the activation energy was greater than the minimum value for semi-insulating SiC substrates. EPR data, measured for six samples cut from the three wafers used for the Hall measurements, revealed a spectrum with the same g-tensor and temperature dependence as that of the positively charged carbon vacancy at the cubic site [43]. Photo-EPR of the carbon vacancy reveals data similar to that shown in figure 8. Thus it is concluded that the centre in these materials represents V_C^+ with a 0/+ level located near the middle of the 4H SiC

band gap. Such observations suggest that V_C may act as the primary defect for compensation. However, at least two additional results indicate that V_C^+ is not the sole compensating level in this material. The concentration of the carbon vacancy after a 1600 °C anneal in one sample was below the detection limit ($<1 \times 10^{12}$ cm^{-3}) and a small amount ($\sim 10^{14}$ cm^{-3}) of boron was observed in the dark. In similar samples, on the other hand, the activation energy changed by no more than 20% after the 1600 °C Ar anneal, and in all cases the value was greater than 1 eV. If V_C were the only compensating defect, the value of E_a would certainly not be greater than 1 eV when the carbon vacancy was removed. As has been suggested by others, the low number of carbon vacancies measured in the as-grown samples, less than 5×10^{14} cm^{-3}, also suggests that additional centres must compensate the excess acceptors thought to be present in some HPSI wafers [13]. Thus, it appears that, although V_C^+ may compensate some of the excess donors, the vacancy cannot be the sole compensating defect in the material.

Another interesting point regarding the Hall and EPR data is the observation of the positive charge state of the carbon vacancy in samples cut from the same wafers for which Hall measurements show activation energies as low as 0.9 eV and n-type behaviour. Although in general the carrier concentration obtained from these high resistivity samples is questionable, by allowing the temperature to stabilize after each measurement a reliable value of the carrier concentration could be extracted from the Hall data in selected samples. The data reveal an E_a of 1.1 eV and n-type conduction, implying that the Fermi level, E_f, in this sample is 1.1 eV below E_c. In the pieces cut from the same wafer, EPR measurements showed the spectra of V_C^+. The significance lies in the fact that the $V_C^{0/+}$ level is thought to be located at E_c–1.8 eV and observation of V_C^+ indicates that the level is empty. Thus, the defect level assignment implies that an unfilled level lies below E_f. This apparent contradiction may be explained by invoking a Franck–Condon shift with a value greater than 0.7 eV (1.8 − 1.1 eV). As discussed earlier, several theoretical studies predict that a large lattice distortion accompanies the ionization of the carbon vacancy [33, 34] and energies as large as 0.8 eV are estimated [38]. Nevertheless, additional studies on a wide variety of samples are necessary to more fully investigate the defect level of $V_C^{+/0}$, activation energies, and defect relaxation in SiC.

Isochronal annealing studies were performed on PVT HPSI SiC to monitor the stability of V_C^+. Samples were subjected to a sequence of 1 h Ar anneals between 600 and 1700 °C [44, 45]. Figure 9 shows the concentration of carbon vacancies (unfilled circles) and boron acceptors (filled circles) as a function of annealing temperature. The data reveal a decrease in the carbon vacancy concentration and an increase in boron at about the same temperature, 1000 °C. Furthermore, within the factor of two experimental error typical of EPR absolute concentration calculations, a one-to-one exchange between B and V_C is observed in the temperature range of 1000–1400 °C. However, above 1400 °C the total amount of boron exceeds that of the carbon vacancies. The concentration of boron acceptors obtained after the 1700 °C anneal is about ten times bigger than the initial concentration of V_C. After the final heat treatment, the EPR spectrum was measured while exposing the sample to light. Sub-band gap illumination (578 nm) of the 1700 °C annealed sample restored the V_C signal to the original intensity and increased the boron spectral lines. The arrows in figure 9 point to the concentrations measured after illumination. The photo-induced EPR results indicate that thermal annealing did not annihilate the carbon vacancies in this sample.

The trend observed between 1000 and 1400 °C and the measurements made after exposure to sub-band gap light highlight several important results. First, carbon vacancies can compensate boron acceptors. Second, the gradual reduction of V_C above 1000 °C is caused by charge exchange with shallow boron acceptors in these samples. Furthermore, the annealing results combined with the photo-induced EPR data taken after the 1700 °C anneal reveal that

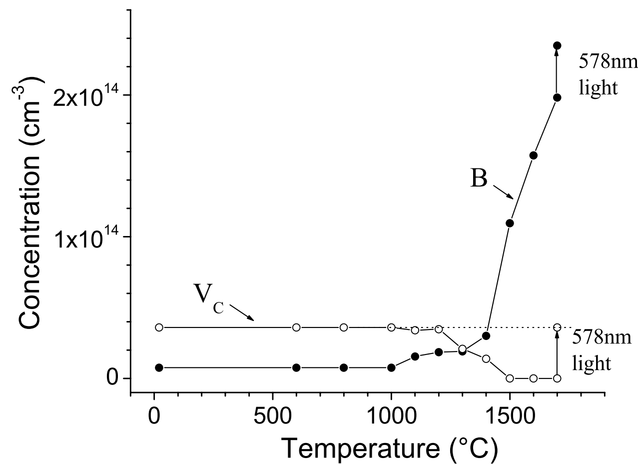

Figure 9. Concentration of V_C^+ (unfilled circles) and shallow B acceptor (filled circles) in 4H SiC as a function of annealing in dry Ar at specified temperature. The arrows show the increase of V_C^+ and B signals during exposure to 578 nm light. (Reprinted from [45], figure 5, with permission of TMS.)

although heat treatment may change the charge state of V_C, the *defect* is thermally stable up to 1700 °C. However, it is cautioned that results like those shown in figure 9 are expected to depend on the amount of both extended and point defects in the crystal. Clearly, additional studies including annealing and photo-induced EPR on a wide variety of samples must be performed before the fundamental annealing kinetics of the carbon vacancy can be definitively established.

The stability of the carbon vacancy is also reported by several other groups [14]. In addition to V_C at the cubic site, the work addresses the stability of V_C at the hexagonal site and V_{Si}.

Unlike V_C, the V_C–C_{Si} pair and V_{Si} require illumination with sub-band gap light to enhance the EPR active state. Thus, photo-induced EPR methods are not a practical approach for estimating the defect level. The deep level nature of the centres may be inferred from the fact that in as-grown material they have been observed only in semi-insulating substrates. In addition, the use of 1.1 eV photons to excite the $S = 1$ state of the $(V_C–C_{Si})^{2+}$ pair suggests that the ground state must be at least 1 eV from either band edge. Thus, the pair appears to be a candidate for the compensating defect in HPSI SiC. The $(V_C–C_{Si})^{2+}$ centre is a particularly interesting candidate because the double-plus charge state and negative-U character imply that it will trap two electrons for every one donor. Unfortunately, the number of defects is difficult to measure because the centre is only observed with illumination. A preliminary study suggested that the concentration may be sufficiently high to provide compensation, but more refined estimates place the defect density significantly below N_d–N_a [46]. Thus, like V_C^+, the pair centre cannot be the sole compensating level in this material. As for the silicon vacancy, theoretical studies have placed the $V_{Si}^{-/0}$ transition between 0.6 and 1.4 eV above the valence band edge [20, 33], but it is not a likely candidate for compensation because annealing studies of electron-irradiated p-type 4H SiC show that the centre may be removed by a 700 °C heat treatment. In fact, the intensity of the V_{Si} EPR signal decreases while that for the V_C–C_{Si} pair increases as the anneal temperature increases [14]. Thus, earlier suggestions that V_{Si} forms the precursor of the pair defects appear to be confirmed. It seems likely that the primary role of the silicon vacancy in the production of HPSI substrates is that of a precursor for the V_C–C_{Si} pair, which compensates at least some of the shallow impurities in the material.

3. Impurity-related defects

This section will first present recent work concerning the aluminium acceptor and phosphorus donors in SiC. Little new information has come forth regarding the other two most common shallow impurities, boron and nitrogen; thus, the reader is left to the several excellent reviews summarizing magnetic resonance studies of these shallow impurities [5, 11, 47]. Also included in this section is vanadium, the deep level impurity commonly used for compensation in SI wafers. The two charges states, V^{4+} and V^{3+}, will be discussed as well as the photo-EPR measurements of their optical transitions.

3.1. Shallow impurities

Several groups have studied the potential of phosphorus as a shallow donor in SiC. Veinger and, separately, Kalabukhova first identified the EPR of phosphorus in 6H SiC doped by neutron transmutation [48, 49]. Two of the signals observed were attributed to P substituting for Si at the hexagonal and cubic lattice sites. The signal was also observed in P-ion implanted SiC [50]. Recently, Isoya and co-workers performed a systematic study of the effects of implantation energy, temperature, and annealing conditions on the shallow phosphorus centres [51]. In samples implanted at 3 MeV and 340 keV at temperatures between room temperature and 1200 °C, the only EPR signals observed are those due to the unintentionally incorporated nitrogen impurities and implantation damage. The amplitude of the latter decreases with increasing implantation temperature. After annealing at 1650 °C for 30 min in Ar, the samples show the characteristic spectra of isolated phosphorus donors. The amount of P donors, which did not vary with implantation temperature, was calculated to be less than 8% of the total implanted phosphorus ions. The small fraction of centres situated on the lattice sites is consistent with the limited success of n-type doping via phosphorus implantation. The remaining phosphorus ions may by associated with the P-related defects reported in SiC:P doped by means of neutron transmutation. However, no spectra similar to those reported by Kalabukhova or Veinger were reported in the more recent studies of ion-implanted material.

Aluminium is the p-type dopant of choice. In contrast to N and B, little is published about EPR-detection of the aluminium acceptor in SiC. The different symmetry sites have not been resolved, but it is known that Al, unlike B, exhibits an EPR response typical of an effective-mass-like shallow acceptor [5]. Photoluminescence detected EPR (PL-EPR) results are consistent with the $E_v + 0.191$ eV level reported for the Al acceptor [5]. However, magnetic-circular dichroism EPR measurements determine the level to be somewhat deeper, 0.25 eV [5]. The concentration and temperature dependence of the Al EPR signal was reported recently by Gerardi [52]. The Al signal monotonically increases with hole concentration; however, only about one-tenth of the holes may be accounted for by the EPR active Al centres in these samples. Studies of the shape of the Al signal reveal additional interesting concentration affects. Intensity and linewidth changes as a function of temperature and concentration are interpreted in terms of site-to-site impurity hopping when the Al concentration is below 1×10^{18} cm^{-3}. Above this value, a broad isotropic line typical of nearly free electrons emerges, prompting the authors to suggest that impurity band conduction dominates.

3.2. Deep level impurity: vanadium

Of the many transition metals identified in SiC by EPR, the most technologically important is vanadium. Vanadium has long been recognized as a deep level defect capable of compensating unintentional acceptors and donors, thereby yielding semi-insulating substrates required for MESFET and HMET devices. Although today vanadium-doped wafers are challenged by the

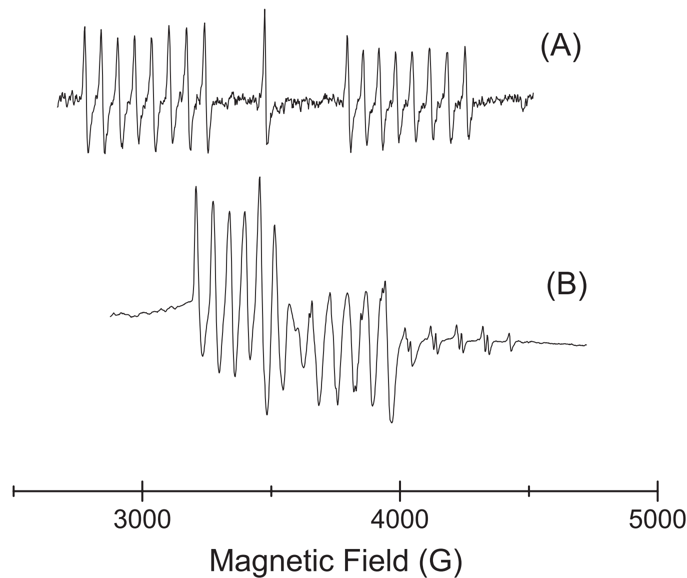

Figure 10. EPR spectra of V^{3+} at the cubic site (a) and V^{4+} and V_x^{4+} (b) of vanadium-doped SI 4H SiC. The spectra were measured at 30 K with B perpendicular to the c-axis (a), and at 4 K with B parallel to the c-axis (b). The sharp line near 3500 G in (a) represents surface damage.

latest innovations in high purity material, for many devices the SI wafers formed by impurity doping remain a viable, and cheaper, alternative. The utility of this d^5 transition element lies in its ability to electrically passivate shallower defects by trapping both electrons and holes. When the vanadium concentration is adjusted appropriately, SiC wafers may be produced with resistivity as high as 10^7 Ω cm at 300 °C.

Two different notations are used to denote the charge states of vanadium, one borrowed from point defects in ionic solids and the other from standard semiconductor terminology. For instance, the equivalent of the 'free atom' neutral charge state is referred to as either V^{4+} or V^0, since four of the five vanadium valence electrons form tetrahedral bonds in SiC. The donor level is written as either $V^{4+/5+}$ or $V^{0/+}$. In deference to the EPR literature, the ionic notation will be used throughout this discussion rather than traditional semiconductor language.

The EPR signatures of the three-plus and four-plus charge states of vanadium, as well as their defect levels, are well studied in both 6H and 4H SiC. The 10 GHz EPR spectra of V^{3+} and V^{4+} measured in SI SiC at 4 K are shown in figures 10(a) and (b), respectively. Only the portion of the V^{3+} spectrum related to the hexagonal site is shown; the spectrum for the cubic site was also observed when a larger magnetic field range was employed. The sharp isolated line near 3480 G represents surface damage from the cut edges of the sample. Analysis of the 'half-field' lines for V^{3+} reveals interactions with Si neighbours consistent with a description of the impurity as substitutional vanadium residing on an Si lattice site [53]. Since V^{3+} is found exclusively in n-type SiC, the $V^{3+/4+}$ level is thought to lie in the upper half of the band gap. A correlation of EPR and optical absorption results places the energy within 0.66 eV of E_c in 6H SiC and about 0.8 eV below E_c in 4H [54, 55].

Eight of the lines at highest magnetic field in the figure 10(b) have approximately the same $g_\parallel$-values and $A_\parallel$-values as V^{4+} at the hexagonal site [6]. The remaining portion of the spectrum, referred to here as V_x^{4+}, is likely related to V^{4+} at the cubic site; however, the

complicated angular dependence suggests that the centre is complexed with another defect. Vanadium centres coupled to separate defects have been proposed by others studying the luminescence and absorption of SiC [56]. Monitoring vanadium on the cubic site in 6H SiC:Al (p-type) as a function of excitation wavelength, Maier and co-workers demonstrated that the $V^{4+/5+}$ level lies 1.6 eV above the valence band edge [6, 53]. In this study, the level for the hexagonal site was not determined.

Recently, photo-EPR studies of vanadium-doped semi-insulating SiC suggest refinements to the reported value of the $V^{3+/4+}$ defect level and identify the donor level for V^{4+} at the hexagonal site [43]. The studies are based on a comparison between the EPR data and carrier activation energies extracted from temperature-dependent Hall measurements. In vanadium-doped SI 4H SiC with a carrier activation energy of 1.6 eV, dark EPR measurements reveal the presence of V^{4+} at both the hexagonal and cubic sites and no evidence of V^{3+}. Optical excitation with photon energy greater than 1.5 eV increases the EPR signal intensity of V^{4+} at both sites, converting V^{5+} to V^{4+} via capture of an electron from the valence band, consistent with similar experiments done by others addressing the cubic site. Thus, the donor level at each symmetry site appears to be about 1.6 eV above E_c. Both the dark and photo-EPR measurements verify that the vanadium impurity is the predominant source of compensation in SI SiC:V wafers with activation energy of 1.6 eV.

In contrast to samples with $E_a = 1.6$ eV, vanadium-doped SiC wafers with a 1.1 eV activation energy reveal the presence of both V^{4+} and V^{3+} when measured in the dark. The presence of both charge states, neutral and negative, in samples for which temperature-dependent Hall measurements yield n-type conduction, and a 1.1 eV activation energy suggests that the Fermi energy lies near the $V^{3+/4+}$ acceptor level and that the level is located 1.1 eV below the conduction band edge. Photo-EPR reveals changes in the concentrations of both V^{4+} and V^{3+} at energies of about 1 eV, offering additional support for locating the acceptor level at $E_c - 1.1$ eV. Interestingly, no change is seen in the intensity of V^{3+} at 0.8 eV as might be expected from the $V^{3+/4+}$ level reported in the literature [55]. The photo-induced EPR data are complicated, but Zvanut and co-workers suggest that an optical threshold at 1.2 eV represents electron excitation from V^{3+} to the conduction band, and corresponds to the 1.1 eV activation energy extracted from temperature-dependent Hall measurements of the same samples. The small difference between the optical threshold energy (1.2 eV) and thermal activation energy (1.1 eV) is attributed to a Franck–Condon shift. The dark EPR spectrum, V^{3+} photo-EPR data, and temperature-dependent Hall results are unchanged after annealing at temperatures as high as 1600 °C, providing additional support for the correlation between the V^{3+} EPR data and Hall data. Unfortunately, the decreases in V^{3+} did not always correspond to equivalent increases in V^{4+} as might be expected for excitation of an electron from V^{3+} to the conduction band, so that verification of the $V^{3+/4+}$ level could not be confirmed. The lack of consistent correlation between V^{3+} and V^{4+} is attributed to contributions by other deep level defects.

4. Surface and interface defects

The surface of SiC is an integral part of transistor-based electronics because the operation of a device often occurs within the top few microns of the wafer. Furthermore, metal–oxide–semiconductor transistors rely on a high quality surface to achieve the best possible SiO_2 layer as well as a low-defect interface. In Si devices, paramagnetic defects at the oxide/Si interface are known to be directly related to electrically active trapping sites that alter device performance [57]. For these reasons, several EPR studies have focused on defects near the surface of SiC wafers as well those in the vicinity of the SiC/SiO_2 interface [58–60]. EPR cannot selectively detect centres at surfaces and interfaces because the microwaves penetrate

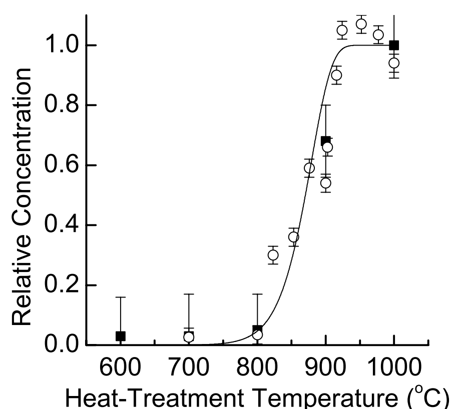

Figure 11. Activation profile for a C-dangling bond centre in oxidized 3C SiC epilayer samples (unfilled circles) and 6H SiC (filled squares). The solid curve represents a fit of the Arrhenius equation to the 3C SiC data from which an activation energy of 4.0 ± 0.3 eV is estimated (with permission of reproduction from the American Institute of Physics).

the entire SiC substrate. For a perfectly flat surface, the angular dependence of the EPR resonance may provide enough information to deduce the surface nature of the centre as was done for the Si P_b centre located at the interface between a (111) Si substrate and amorphous SiO_2 layer [61]. Usually, however, identification of an EPR spectrum with a surface is based on etching studies that involve monitoring the intensity of the EPR signal as thin layers of the material are removed. Below, two types of studies are reviewed. The first addresses the affect of annealing temperature and ambient on a defect believed to be located near the surface of SiC. The second focuses on a defect in oxidized porous SiC, which is proposed as the SiC analogue of the Si P_b centre.

4.1. Heat-treated surfaces

Room temperature EPR studies of as-grown SiC wafers usually reveal an isotropic line with g-values ranging between 2.0024 and 2.0026 in 4H SiC [40, 41]. Comparison with similar EPR spectra in intentionally damaged and amorphous SiC suggests that the defect is a C-dangling bond. A series of annealing and etching studies were performed on this centre to obtain a basic understand of the chemistry of the defect as well to determine the location of the centre. In one study, the defect was examined by first oxidizing SiC in steam at 1150 °C for 6 h to eliminate the centre [41]. The samples were then heat-treated in dry N_2 (99.999% pure) for 200 min at 900 °C. In the three polytypes studied, 3C, 6H, and 4H, the signal was quenched by the oxidation and regenerated by the heat treatment. The relative amplitude of the EPR signal measured after thermal treatment in N_2 at different temperatures is shown in figure 11 for 3C (unfilled circles) and 6H SiC (filled squares). The maximum total number of centres is of the order of 10^{12}. The results were interpreted in terms of removal of hydrogen from a C-dangling bond. The activation energy calculated from these data, 4.0 ± 0.3 eV, is consistent with the expected strength of a C–H bond, supporting the defect depassivation interpretation.

After generating the C-dangling bond signal, the samples were subjected to a series of anneals in forming gas (H_2/N_2) at temperatures up to 700 °C [41]. Figure 12 shows the results for both the undoped 3C (unfilled circles) and p-type 6H SiC (filled squares). It is thought that the difference in energy required to re-passivate the centres is related to the dependence of hydrogen diffusivity on resistivity rather than polytype. In summary, the activation/passivation

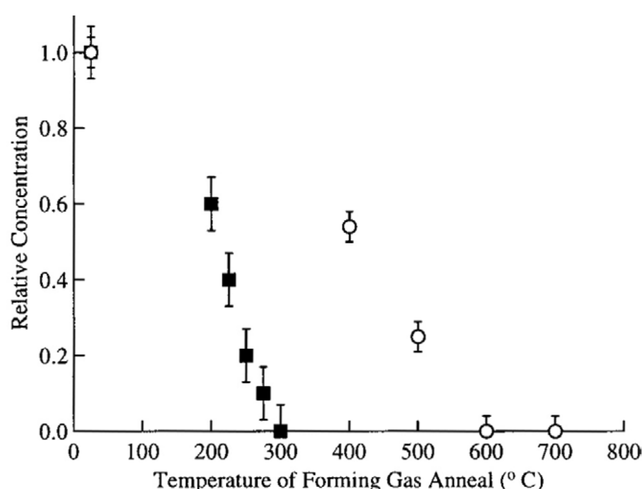

Figure 12. The concentration of C-dangling bond centre in oxidized dry heat-treated 6H (filled squares) and 3C (unfilled circles) SiC as a function of forming gas (7% H_2 and 93% N_2) annealing temperature (with permission of reproduction from the American Institute of Physics).

study suggests that the C-dangling bond in SiC may be 'cured' by a low temperature (<700 °C) forming gas anneal but the passivation is not stable. Thermal treatments at temperatures greater than 800 °C release the hydrogen, regenerating the dangling bond defect.

The surface nature of the centre was determined by a series of etching experiments, in which first the oxide, then layers of SiC were sequentially removed [58]. The EPR intensity did not change until all of the oxide had been removed, indicating that the defects are located in the SiC or near the SiC/oxide interface. A similar result was found by Gerardi and co-workers [40]. The depth distribution below the SiC surface was measured using a series of oxidations to remove layers of SiC. The amount of centres observed after at least 1 μm of SiC was removed was within a factor of two of the original number of defects. This result suggests that the centres are not located at the abrupt SiC/SiO_2 interface; rather, the C-dangling bonds are distributed throughout the thickness of the wafer. However, the authors also point out that the oxidation itself may generate the defect. Thus, the work offers two possible scenarios: the defects are incorporated throughout the bulk during growth or they are generated near the surface during oxidation. Note that if the 10^{12} defects measured after each oxidation/heat treatment are distributed uniformly throughout the wafer, the density of these dangling bonds is less than 2×10^{13} cm^{-3}. However, if the centres are generated during oxidation and only those within the maximum estimated 1μm diffusion depth of hydrogen are seen, the density may be as high as 10^{16} cm^{-3}, similar to a typical doping concentration. Whichever situation applies, the presence of C-dangling bonds near the surface or distributed throughout the bulk should not be ignored in the analysis of defects affecting device performance.

4.2. *SiC/SiO_2 interface*

Many EPR studies have identified a dangling bond defect located at the semiconductor–oxide interface [57, 59–63]. Several such defects are found in silicon-based interfaces, each involving an unpaired electron on an Si atom located on the silicon side of the interface [57, 61]. An analogous centre is seen in SiGe–oxide interfaces [62, 63]. The dangling-bond-like defects are referred to collectively as P_b centres. In studies of Si, oxidized planar wafers as well as oxidized porous material were used to study the defect. The latter enhances the surface area,

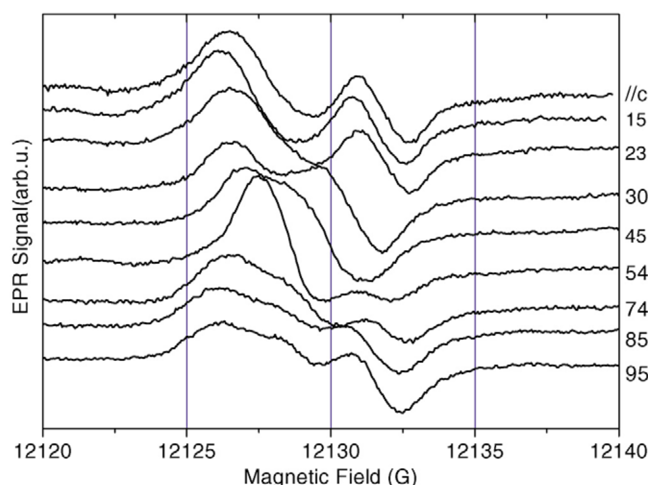

Figure 13. 35 GHz EPR spectra of oxidized porous SiC measured at different angles between the magnetic field and c-axis when the sample is rotated about the $[11\bar{2}0]$ axis. (Reprinted figure with permission from Cantin *et al* [60], copyright 2003 by the American Physical Society).

but lacks the simple symmetry of a planar surface from which the interfacial nature may be directly determined. A study of oxidized planar 6H SiC using spin-dependent recombination reveals a defect reported to be located at or near the SiC/oxide interface, but no further structural information is available [64]. Through a series of oxidation, annealing, and etching studies of oxidized porous SiC, Cantin and co-workers present a convincing case for the observation of a C-dangling bond at the SiC/SiO_2 interface [59, 60]. The defect is named P_{b-c}.

Figure 13 shows 35 GHz EPR spectra of oxidized porous SiC measured at different angles between the magnetic field and c-axis when the sample is rotated about the $[11\bar{2}0]$ axis. The sample consisted of 5–100 μm thick porous SiC layers prepared electrochemically from n-type 4H SiC wafers cut 3.5 or 8$''$ off axis. The oxide was formed by passing dry O_2 over the samples in a furnace at 1000 °C and 23 mbar pressure. The spectrum is deconvoluted into one isotropic line and several anisotropic lines. The former is thought to be associated with carbon trapped in the amorphous SiO_2 layer. The angular dependence of the spectrum indicates that the latter may be interpreted as two defects, one which is axially symmetric about the c-axis and the other pointing along one of the remaining three bonding directions. The g-tensor for each is provided in table 1. For a perfectly planar (0001) surface rotated with the c-axis in the plane of the magnetic field, only one line should be observed at each orientation. The presence of the additional EPR lines is thought to arise from the contribution of a second plane at the porous SiC surface. Such a phenomenon is similar to what is observed for P_{b0}, one of the Si-dangling bonds at the (100) Si/SiO_2 interface [61]. The interfacial nature of the defect is also supported by etching studies, which show that the intensity of the anisotropic spectral lines decrease only gradually with a 60 s soak in a hydrofluoric acid solution, which should not affect the SiC.

Hyperfine interactions from both the nearest neighbour Si atoms as well as the central carbon atom are listed in table 1 [60]. Significantly, the ^{29}Si hyperfine reflects contributions from only 3 Si atoms, as would be expected from a surface centre. The small deviation of $g_{\|}$ from the free electron g-value further supports the description as a carbon-related centre. Spin–orbit coupling shifts the g-value of a defect in a crystal from that found for a free electron by an amount proportional to the spin–orbit coupling constant. g_z for the Si P_b is greater than that for the P_{b-c}, consistent with the relative values of the coupling constant for Si and C.

The above studies provide strong evidence for the presence of P_b-like defects at the surface of oxidized SiC. Unfortunately, the need to deconvolute the spectra inevitably limits the accuracy of results such as the number of nuclei contributing to the hyperfine spectrum. Also, although the presence of dangling bonds along a direction other than the *c*-axis is expected for porous material, the observation inhibits firm conclusions regarding the interfacial nature. Ultimately, one would like to detect the centres at the planar surface of (0001) SiC, where a single resonance line exhibiting axial symmetry about the *c*-axis is expected. However, the quality of SiC surfaces to date and the signal-to-noise difficulties inherent in EPR studies of interfaces suggest that definitive confirmation of an interfacial centre at the SiC/SiO_2 interface will be challenging, at the very least.

5. Concluding comments

The previous pages have reviewed EPR studies of SiC, primarily focusing on SI SiC. The intrinsic defects observed to date in as-grown high purity SI SiC were described and a variety of processes related to impurities in n-type, p-type, and compensated wafers was addressed. Several other issues should be mentioned regarding future magnetic resonance studies of SiC. First, in order to accurately describe any defect, the full symmetry of the centre should be determined. Such studies require rotation of the sample about three mutually perpendicular axes, a situation difficult to realize when confined to mm-thick wafers. Thus, bulk electronic grade samples would enhance our knowledge of many of the defects discussed above. The use of thicker pieces would also address another problem, signal-to-noise ratio. The high quality of the material now being produced for device applications severely minimizes the amount of point defects detectable by EPR. Often, the limited sample size afforded by the thin wafers is overcome by stacking several pieces; however, this can lead to misalignment of the crystal axis and produce artificially complicated line shapes.

Another problem that plagues many defects in SiC is the similarity of the g-tensor found among many intrinsic EPR centres. This factor is inherent to SiC because the shift of g from the free electron value is proportional to the spin–orbit coupling constant, a value that is small for both C and Si. Thus, several different intrinsic defects may be barely resolved at the typical measurement frequency of 10 GHz. Lately, this problem has been addressed by experiments employing frequencies as high as 240 GHz. Although the complexity of such experiments limits their potential as routine characterization methods, the intensive studies have resolved spectra of several intrinsic defects in as-grown SI SiC and have provided valuable structural information [4, 31, 32].

It is hoped that this review highlights the significance of EPR to point defect studies and furthers the understanding of defect-related phenomena.

Acknowledgments

This work is funded by Dr Colin Wood, US Office of Naval Research. The author gratefully acknowledges the assistance of Dr V Konovalov, Ms Hiayan Wang, and Mr D Alvarez for acquisition of some of the data reported here. Helpful discussions with Drs W Carlos, M Bockstedte, and W Mitchel are also sincerely acknowledged.

References

[1] Poole C P 1967 *Electron Spin Resonance: A Comprehensive Treatise on Experimental Technique* (New York: Interscience)
[2] Gordy W 1980 *Techniques of Chemistry* vol 15, ed W West (New York: Wiley)

[3] Weil J A, Bolton J R and Wertz J E 1994 *Electron Paramagnetic Resonance* (New York: Wiley)
[4] Konovalov V V, Zvanut M-E and van Tol J 2003 *Phys. Rev.* B **68** 012102
[5] Greulich-Weber S 1997 *Phys. Status Solidi* a **182** 95
[6] Maier K, Schneider J, Wilkening W, Leibenzeder S and Stein R 1992 *Mater. Sci. Eng.* B **11** 27–30
[7] Zvanut M E and Konovalov V V 2002 *Appl. Phys. Lett.* **80** 410
[8] Son N T, Magnusson B and Janzen E 2003 *Appl. Phys. Lett.* **81** 3945–7
[9] Balona L A de S and Loubser J H N 1970 *J. Phys. C: Solid State Phys.* **3** 2344
[10] Itoh H, Kawasuso A, Ohshima T, Yoshikawa M, Nashiyama I, Tanigawa S, Misawa S, Okumura H and Yoshida S 1997 *Phys. Status Solidi* a **162** 173
[11] Schneider J and Maier K 1993 *Physica* B **185** 199
[12] Baur J, Kunzer M and Schneider J 1997 *Phys. Status Solidi* a **162** 153
[13] Carlos W E, Glaser E R and Shanabrook B V 2003 *Physica* B **340–342** 151
[14] Zolnai Z, Son N T, Magnusson B, Hallin C and Janzen E 2004 *Mater. Sci. Forum* **457–460** 473
[15] Mizuochi N, Yamasaki S, Takizawa H, Morishita N, Ohshima T, Itoh H and Isoya J 2002 *Phys. Rev.* B **66** 235202
[16] Orlinski S B, Schmidt J, Mokhov E N and Baranov P G 2003 *Phys. Rev.* B **67** 125207
[17] Wimbauer T, Meyer B K, Hofstaetter A, Scharmann A and Overhof H 1997 *Phys. Rev.* B **56** 7384
[18] Son N T, Zolnai Z and Janzen E 2003 *Phys. Rev.* B **64** 205211
[19] Sorman E, Son N T, Chen W M, Kordina O, Hallin C and Janzen E 2000 *Phys. Rev.* B **61** 2613
[20] Zywietz A, Furthmuller J and Bechstedt F 1999 *Phys. Rev.* B **59** 15166
[21] von Bardeleben H J, Cantin J L and Vickridge I 2000 *Phys. Rev.* B **62** 10126
[22] Itoh H and Hayakawa N 1989 *J. Appl. Phys.* **66** 4529
[23] Lingner Th, Greulich-Weber S and Spaeth J-M 2001 *Phys. Rev.* B **64** 245212
[24] Vainer V S and Il'in V A 1981 *Sov. Phys.—Solid State* **23** 2126
[25] Son N T, Hai P N, Wagner Mt, Chen W M, Ellison A, Hallin C, Monemar B and Janzen E 1999 *Semicond. Sci. Technol.* **14** 1141
[26] Konovalov V V, Zvanut M E, Jenny J R, Müller S G, Hobgood H McD and Tsvetkov V 2002 *Physica* B **308–310** 671
[27] Son N T, Hai P N and Janzen E 2001 *Phys. Rev.* B **63** 201201
[28] Bratus V Ya, Makeeva I N, Okulov S M, Petrenko T L, Petrenko T T and von Bardeleben H J 2001 *Physica* B **308–310** 621
[29] Bockstedte M, Heid M and Pankratov O 2003 *Phys. Rev.* B **67** 193102
[30] Petrenko T T, Petrenko T L, Bratus V Ya and Monge J L 2001 *Physica* B **310** 637
[31] Son N T, Hai P N and Janzen E 2001 *Phys. Rev. Lett.* **87** 045502
[32] Umeda T, Isoya J, Morishita N, Ohshima T and Kamiya T 2004 *Phys. Rev.* B **69** 121201
[33] Bechstedt F, Fissel A, Furthmuller F, Grossner U and Zywietz A 2001 *J. Phys.: Condens. Matter* **13** 9027–37
[34] Torpo L, Marlo M, Staab T E M and Nieminen R M 2001 *J. Phys.: Condens. Matter* **13** 6203–31
[35] Konovolova V V and Zvanut M E 2003 unpublished
[36] Konovalov V V and Zvanut M E 2002 *J. Electron. Mater.* **31** 351
[37] Kalabukhova E N, Lukin S N, Saxler A, Mitchel W C, Smith S R and Solomon J S 2001 *Phys. Rev.* B **64** 235202
[38] Bockstedte M 2004 private communication
[39] Son N T, Magnusson B, Zolnai Z, Ellison A and Janzen E 2003 *Mater. Sci. Forum* **433–436** 45
[40] Gerardi G J, Poindexter E H and Keeble D J 1996 *Appl. Spectrosc.* **50** 1428
[41] Macfarlane P J and Zvanut M E 2000 *J. Appl. Phys.* **88** 4122
[42] Mitchel W C, Mitchell W D, Zvanut M E and Landis G 2004 *Solid-State Electron.* at press
[43] Zvanut M E, Konovalov V V, Mitchel W C and Mitchell W D 2004 *Silicon Carbide and Related Materials 2003* (Switzerland: Trans. Tech. Publications) p 489
[44] Alvarez D, Konovalov V V and Zvanut M E May 2002 *State-of-the-Art Program on Compound Semiconductors XXXVI and Wide Bandgap Semiconductors for Photonic and Electronic Devices and Sensors II Electrochemical Society Conf. Proc. 2002–3* ed R F Kopf, F Ren, E B Stokes, H M Ng, A G Baca, S J Pearton and S N G Chu (Pennington, NJ: Electrochemical Society) pp 258–65
[45] Alvarez D, Konovalov V V and Zvanut M E 2003 *J. Electron. Mater.* **32** 444
[46] Carlos W 2003 private communication
[47] Baranov P G 1997 *Defect Diff. Forum* **148/149** 129
[48] Veinger A I, Zabrodskii A G, Lomakina G A and Mokhov E N 1986 *Sov. Phys.—Solid State* **28** 917
[49] Kalabukhova E N, Lukin S N and Mokhov E N 1993 *Sov. Phys.—Solid State* **35** 361
[50] Kalabukhova E N, Lukin S N, Mokhov E N, Feege M, Greulich-Weber S and Spaeth J-M 1993 *Inst. Phys. Conf. Ser.* **137** 215
[51] Isoya J, Ohshima T, Ohi A, Morishita N and Itoh H 2003 *Nucl. Instrum. Methods* B **206** 965

[52] Gerardi G J, Poindexter E H and Keeble D J 2000 *J. Appl. Phys.* **87** 1914
[53] Maier K, Muller H D and Schneider J 1992 *Mater. Sci. Forum* **81–87** 1183–94
[54] Kunzer M, Kaufmann U, Maier K and Schneider J 1995 *Mater. Sci. Eng.* B **29** 118
[55] Jenny J R, Skowronski M, Mitchel W C, Hobgood H M, Glass R C, Augustine G and Hopkins R H 1996 *J. Appl. Phys.* **68** 1963
[56] Dornen A, Latushko Y, Suttrop W, Pensl G, Leibenzeder S and Stein R 1992 *Mater. Sci. Forum* **83–87** 1213
[57] Poindexter E H and Caplan P J 1981 *J. Appl. Phys.* **52** 679
[58] Macfarlane P J and Zvanut M E 1999 *Mater. Sci. Forum* **338–342** 1125
[59] von Bardeleben H J, Cantin J L, Mynbaeva M, Saddow S E, Shishkin Y, Devaty R P and Choyke W J 2003 *Electrochem. Soc. Proc.* **2003/02** 39
[60] Cantin J L, von Bardeleben H J, Shishkin Y, Ke Y, Devaty R P and Choyke W J 2004 *Phys. Rev. Lett.* **92** 015502
[61] Caplan P J, Poindexter E H, Deal B E and Razouk R R 1979 *J. Appl. Phys.* **50** 5847
[62] Cantin J L, Schoisswohl M, von Bardeleben H J, Morazzani V, Ganem J J and Trimaille I 1996 EPR study of the defects in porous Si/SiO_xN_y and $Si_{0.80}Ge_{0.20}$/$SiGeO_2$ *The Physics and Chemistry of SiO_2 and Si/SiO_2 Interfaces* vol 96-1, ed H Z Massoud, E H Poindexter and C R Helms (Pennington, NJ: The Electrochemical Society) p 28
[63] Zvanut M E, Carlos W E, Paine D C and Caragianis C 1993 *Appl. Phys. Lett.* **63** 3049
[64] Meyer D J, Bohna N A, Lenahan P M and Lelis A J 2004 *Appl. Phys. Lett.* **85** 3406